

Spinodal density enhancements in simulations of relativistic nuclear collisions

Jan Steinheimer* and Jørgen Randrup

Nuclear Science Division, Lawrence Berkeley National Laboratory, Berkeley, California 94720, USA

(Dated: October 9, 2012)

We recently introduced a fluid-dynamical model for simulating relativistic nuclear collisions in the presence of a first-order phase transition and made explorative studies of head-on lead-lead collisions. We give here a more detailed account of this novel theoretical tool and carry out more exhaustive studies of the phase-separation dynamics. Extracting the density enhancement caused by the spinodal instabilities, the associated clump size distribution, and the resulting transverse flow velocity, we examine the sensitivity of these quantities to the strength of the gradient term that promotes the phase separation, to the details of the initial density fluctuations that form the seeds for the subsequent amplification, and to the equation of state.

PACS numbers: 25.75.-q, 47.75.+f, 64.75.Gh, 81.30.Dz

I. INTRODUCTION

The aim of high-energy nuclear physics is to elucidate the properties of strongly interacting matter at extreme temperatures and densities. A central subject in these investigations is the quark-gluon plasma (QGP), a new phase of matter in which the quarks and gluons are deconfined. Experiments at SPS, RHIC, and LHC have produced vast amounts of data indicating that such a new phase is indeed produced [1–11].

Strongly interacting matter is expected to possess a rich phase structure. In particular, compressed baryonic matter may exhibit a first-order phase transition that persists up to a certain critical temperature [12]. At vanishing baryon chemical potential, lattice QCD calculations yield a smooth transformation from confined to deconfined matter at a cross-over temperature of $T_{\times} \approx 150 - 160$ MeV [13, 14]. Unfortunately, the lattice calculations cannot be readily extended to finite chemical potential due to the so-called sign problem. While several methods have been employed for circumventing this basic problem, including Taylor expansion in μ/T , reweighting, and imaginary chemical potential, the results are not conclusive on the existence of a genuine first-order phase transition at finite chemical potential and the location of the associated critical point [15–18].

It is therefore necessary to rely on experiment for the determination of the phase structure of baryon-rich strongly interacting matter. Experimental efforts are underway to search for evidence of a first-order phase transition and the associated critical end point [19–21]. For these endeavors to be successful, it is important to identify observable effects that may serve as signals of the phase structure. This is a challenging task because the colliding system is relatively small, non-uniform, far from global equilibrium, and rapidly evolving, features that obscure the connection between experimental observables and the idealized uniform equilibrium matter described

by the equation of state. Therefore, to understand how the presence of a phase transition may manifest itself in the experimental observables, it is necessary to carry out dynamical simulations of the collisions with suitable transport models.

Many numerical simulations of high-energy nuclear collisions have employed ideal or viscous fluid dynamics which has the important advantage that the equation of state (EoS) appears explicitly. By contrast, in most microscopic transport models the EoS is often unknown or very cumbersome to determine. The focus up to now has mainly been on bulk observables and their dependence on a softening of the EoS. For this purpose, the instabilities associated with a first-order phase transition were usually removed by means of a Maxwell construction, thereby ensuring that bulk matter remains mechanically stable throughout the expansion.

However, when a first-order phase transition exists, a low-density confined phase (a hadronic resonance gas) may coexist thermodynamically with a high-density deconfined phase (a baryon-rich quark-gluon plasma) and, consequently, bulk matter prepared at intermediate densities would be unstable and seek to separate into the two coexisting phases. Therefore, in a nuclear collision, when the dynamical evolution drives the bulk density into the phase coexistence region, the instabilities will be triggered. In particular, the spinodal instabilities [22–25] may generate a non-equilibrium evolution that in turn may generate observable fluctuations in the baryon density [26–29] and the chiral order parameter [30, 31]. Furthermore, nucleation and bubble formation may also contribute towards the phase separation process.

In order to ascertain the degree to which these mechanisms may manifest themselves in actual nuclear collisions, we have performed numerical simulations with finite-density fluid dynamics, using a previously developed two-phase equation of state and incorporating a gradient term in the local pressure [32]. This latter refinement emulates the finite-range effects that are essential for a proper description of the phase transition physics [22, 23, 25, 33]. In particular, the gradient term ensures that two coexisting bulk phases will develop a diffuse in-

* jsfroschauer@lbl.gov

interface and acquire an associated temperature-dependent tension. Furthermore, of key importance to the present study, the gradient term also causes the dispersion relation for the collective modes in the unstable phase region to exhibit a maximum, as is a characteristic feature of spinodal decomposition [22]. Thus we employ a transport model that has an explicitly known two-phase equation of state and that treats the associated physical instabilities in a numerically reliable manner.

A first application of this novel tool was recently made for head-on collisions of lead nuclei at various energies [32]. For a certain range of collision energies, several GeV per nucleon, the bulk of the system will reside within the spinodal region of the phase diagram for a sufficient time to allow the associated instabilities to significantly enhance the initial density irregularities. This characteristic phenomenon was exploited previously to obtain experimental evidence for the nuclear liquid-gas phase transition [22, 34] and we are exploring the prospects for it being useful for signaling the confinement phase transition.

II. THE EQUATION OF STATE

In order to obtain a suitable equation of state, we employ the method developed in Ref. [25]. Thus we work (at first) in the canonical framework and, for a given T , we obtain the free energy density $f_T(\rho)$ in the phase coexistence region by performing a suitable spline between two idealized systems (either a gas of pions and interacting nucleons or a bag of gluons and quarks) held at that temperature. In Ref. [25] the focus was restricted to subcritical temperatures, $T < T_{\text{crit}}$, so for each T the spline points were adjusted so the resulting $f_T(\rho)$ would exhibit a concave anomaly, *i.e.* there would be two densities, $\rho_1(T)$ and $\rho_2(T)$, for which the tangent of $f_T(\rho)$ would be common. This ensures phase coexistence, *i.e.* the chemical potentials match, $\mu_T(\rho_1) = \mu_T(\rho_2)$, because $\mu_T(\rho) = \partial_\rho f_T(\rho)$, and so do the pressures, $p_T(\rho_1) = p_T(\rho_2)$, because $p_T(\rho) = \mu_T(\rho)\rho - f_T(\rho)$. Ref. [32] extended the equation of state to $T > T_{\text{crit}}$ by using splines that are convex, as is characteristic of single-phase systems. After having thus constructed $f_T(\rho)$ for a sufficient range of T and ρ , we may obtain the pressure, as well as the energy density $\varepsilon_T(\rho) = f_T(\rho) - T\partial_T f_T(\rho)$, by suitable interpolation and then tabulate the equation of state, $p_0(\varepsilon, \rho)$, on a convenient Cartesian lattice. The procedure is illustrated in Fig. 1.

Figure 2 shows a contour plot of the resulting equation of state in the canonical representation, $p_T(\rho)$. The lower and upper boundaries of the phase coexistence region, $\rho_1(T)$ and $\rho_2(T)$, respectively, are shown; they come together at the critical point $(\rho_{\text{crit}}, T_{\text{crit}})$. Uniform matter is thermodynamically unstable inside this region, but still mechanically stable near the phase coexistence boundaries. But inside the spinodal boundary, along which the speed of sound vanishes, uniform matter is both thermo-

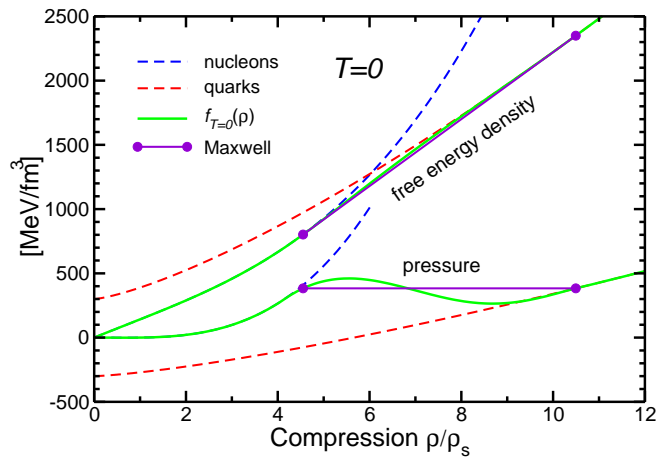


FIG. 1. [Color online] The construction of the equation of state is illustrated for $T = 0$. *Top part:* The free energy densities for either an interacting nucleon gas or quarks in a bag are joined by a spline, yielding a free energy density $f_{T=0}(\rho)$ (solid curve) having a concave anomaly, as is characteristic of a first-order phase transition. The single-phase partner $f_T^M(\rho)$ results when $f_T(\rho)$ is replaced by the common tangent in the coexistence density region. *Bottom part:* The corresponding plot for the pressure $p_T(\rho)$, which exhibits an undulation through the coexistence region where its Maxwell partner $p_T^M(\rho)$ remains equal to the coexistence pressure.

dynamically and mechanically unstable so, consequently, arbitrarily small density irregularities are amplified at a scale-dependent rate $\gamma_k(\rho, T)$.

It is important to recognize that the introduction of the gradient term ensures that our model describes the instabilities not only in the unstable spinodal region, but also those in the surrounding metastable region in which finite seeds are required for amplification to occur (yielding nucleation or bubble formation [28]). Thus density irregularities may be amplified by the metastable region as well, and any clumping generated inside the spinodal region may be further enhanced as the system expands through the nucleation region.

When the dynamical evolution is governed by ideal fluid dynamics (see below) the spinodal boundary is characterized by the vanishing of the isentropic sound speed, $v_s = 0$, where $v_s^2 \equiv (\rho/h)(\partial p/\partial \rho)_{s/\rho}$, with s being the entropy density and $h = p + \varepsilon$ the enthalpy density. For dissipative evolutions the finite heat conductivity causes the instability region to widen and the boundary is then characterized by the vanishing of the isothermal sound speed, $v_T = 0$, where $v_T^2 \equiv (\rho/h)(\partial p/\partial \rho)_T \leq v_s^2$. These spinodal boundaries are also indicated on Fig. 2.

A. Single-phase equation of state

In order to ascertain the dynamical effects of the first-order phase transition, we construct a one-phase partner equation of state that resembles the two-phase equation

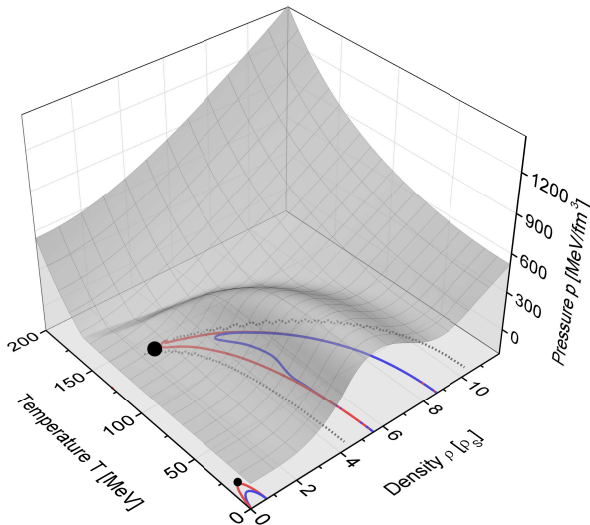


FIG. 2. [Color online] The canonical equation of state $p_T(\rho)$ constructed by a spline procedure, as described in the text. The phase-coexistence boundaries (dotted lines) join at the critical point (solid dot). Also shown are the isothermal spinodal boundary where $v_T=0$ (red) and the isentropic spinodal boundary where $v_s=0$ (blue). The familiar nuclear liquid-drop phase transition occurs at sub-saturation densities, while the confinement transition occurs at densities well above the saturation value ρ_s .

of state as much as possible. Therefore no changes are made outside the phase coexistence region, but for each subcritical temperature $T < T_{\text{crit}}$ the two-phase free energy density $f_T(\rho)$ is replaced by the value obtained by performing a Maxwell construction through the coexistence density region, *i.e.* for $\rho_1(T) < \rho < \rho_2(T)$, namely

$$f_T^M(\rho) = f_T(\rho_i) + (\rho - \rho_i)\mu(\rho_i) < f_T(\rho) . \quad (1)$$

We note this construction lowers the free energy density. This procedure is also illustrated in Fig. 1.

Thus, at a given subcritical temperature T , the chemical potential remains constant when the density is increased from $\rho_1(T)$ to $\rho_2(T)$, because μ_T is the slope of $f_T^M(\rho)$ which is linear. It then follows that also the pressure $p = \mu\rho - f$ remains constant because it is linear in ρ and matches at $\rho = \rho_i$, $f_T^M(\rho_i) = f_T(\rho_i)$ for $i = 1, 2$.

III. FLUID DYNAMICAL CLUMPING

For our present investigation, we describe the evolution of the colliding system by ideal fluid dynamics, because dissipative effects are not expected to play a decisive role for the spinodal clumping [33]: Although the inclusion of viscosity generally tends to slow the growth, the dissipative mechanisms responsible for the viscous effects also lead to heat conduction which has the opposite effect and

also enlarges the unstable region (from the isentropic to the isothermal boundary).

The basic equation of motion in ideal fluid dynamics expresses four-momentum conservation, $\partial_\mu T^{\mu\nu} = 0$, where the stress tensor is given by

$$T^{\mu\nu}(x) = [p(x) + \varepsilon(x)]u^\mu(x)u^\nu(x) - p(x)g^{\mu\nu} , \quad (2)$$

where $u^\mu(x)$ is the four-velocity of the fluid. When taking account of the baryon current density,

$$N^\mu(x) = \rho(x)u^\mu(x) , \quad (3)$$

the basic equation of motion is supplemented by the continuity equation, $\partial_\mu N^\mu = 0$. These equations of motion are solved by means of the code SHASTA [35] in which the propagation in the three spatial dimensions is carried out consecutively.

As mentioned above, a proper description of spinodal decomposition requires that finite-range effects be incorporated [22, 23]. Therefore, following Refs. [25, 33], we write the local pressure as

$$p(\mathbf{r}) = p_0(\varepsilon(\mathbf{r}), \rho(\mathbf{r})) - a^2 \varepsilon_s \frac{\rho(\mathbf{r})}{\rho_s} \nabla^2 \frac{\rho(\mathbf{r})}{\rho_s} , \quad (4)$$

where we recall that $p_0(\varepsilon, \rho)$ is the equation of state, the pressure in uniform matter characterized by ε and ρ . With $\rho_s = 0.153/\text{fm}^3$ being the nuclear saturation density and $\varepsilon_s \approx m_N \rho_s$ the associated energy density, the gradient term is normalized such that its strength is conveniently governed by the length parameter a .

A. Interface tension

As for the pressure (see Eq. (4) above), the free energy density is also modified by the presence of the gradient term. At a given global temperature T , its local value is always increased,

$$f(\mathbf{r}) = f_T(\rho(\mathbf{r})) + \frac{1}{2} a^2 \varepsilon_s \left(\nabla \frac{\rho(\mathbf{r})}{\rho_s} \right)^2 , \quad (5)$$

where $f_T(\rho)$ is the free energy density in uniform matter at the specified density ρ and temperature T . Thus sharp changes in the density are costly and, consequently, if two coexisting phases of bulk matter are brought into physical contact a diffuse interface develops between them. This feature is obviously of key importance for determining the geometric properties of mixed-phase configurations, such as the preferred size of droplets or bubbles. Generally, the equilibrium density can be determined by minimizing the total free energy, subject to conservation of the total baryon number,

$$\delta \int [f(\mathbf{r}) - \mu\rho(\mathbf{r})] d\mathbf{r} \doteq 0 , \quad (6)$$

where μ is the coexistence value of the chemical potential.

The crucial quantity is the tension associated with the interphase between the two coexisting bulk regions. This quantity is most easily determined by considering a planar interface, in which case the above variational condition, after insertion of the form in (5), yields [25]

$$a^2 \frac{\varepsilon_s}{\rho_s^2} \frac{\partial^2}{\partial x^2} \rho(x) = \mu_T(\rho(x)) - \mu = \left[\frac{\partial}{\partial \rho} \Delta f(\rho) \right]_{\rho=\rho(x)}, \quad (7)$$

where the “depth” x is measured in the direction normal to the interface and $\mu_T(\rho)$ denotes the chemical potential in uniform matter at the specified density ρ and temperature T . Furthermore, in the last expression we have used the relation $\mu_T = \partial_\rho f_T$ to introduce the quantity $\Delta f(\rho) \equiv f_T(\rho) - f_T^M(\rho)$, the difference between the actual free energy density at the specified density and that associated with the corresponding Maxwell construction; it is negative for the relevant densities (those between the two coexistence densities).

The solution of the above differential equation (7) yields the diffuse equilibrium density profile $\rho(x)$ which changes smoothly from one coexistence value to the other as x moves through the interface region. However, due to the simplicity of the gradient approximation, the associated interface tension can readily be determined from the equation of state alone, without explicit knowledge of $\rho(x)$ [25], namely

$$\sigma_T = a \int_{c_1(T)}^{c_2(T)} [2\varepsilon_s \Delta f_T(c)]^{1/2} dc, \quad (8)$$

where $c \equiv \rho/\rho_s$ denotes the degree of compression. At the specified sub-critical temperature T , the integral extends over compressions in the corresponding coexistence region. The interface tension σ_T decreases steadily as T is raised and finally vanishes at T_{crit} . It is therefore convenient to characterize it by its maximum value, $\sigma_{T=0}$.

Generally the tension between two coexisting phases plays a key role in determining the characteristic spatial scale of the phase mixture that results when matter prepared in the unstable spinodal region phase separates. Unfortunately, the strength of the tension between nuclear and quark matter is not well understood and the literature contains a large spread of suggested values. For our present studies we have adjusted the range a so that $\sigma_0 \approx 10 \text{ MeV/fm}^2$, which is obtained for $a = 0.033 \text{ fm}$. (For comparison the surface tension of nuclear matter is $\approx 1 \text{ MeV/fm}^2$.) Though this value lies in the lower part of the range, it was preferred in a related study [28] and agrees with the value of the surface tension found for the Polyakov-Quark-Meson model [36] (see also the discussions in Refs. [37, 38], for example).

B. Spinodal amplification

As mentioned above, uniform matter inside the spinodal region (where $v_s^2 < 0$) is mechanically unstable and

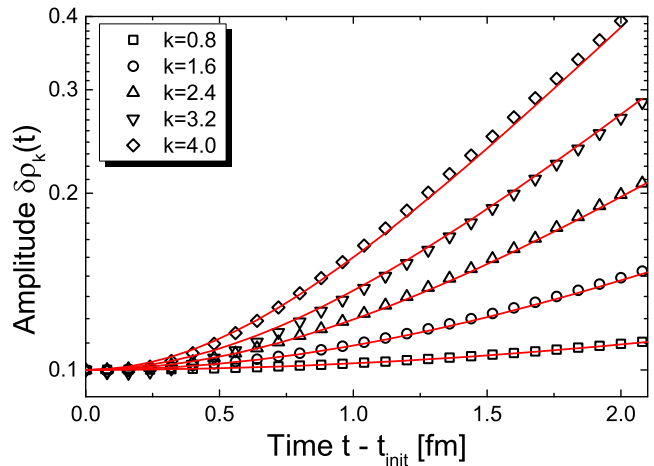


FIG. 3. [Color online] The growth of harmonic density undulations inside the spinodal region as obtained with standard ideal fluid dynamics, shown by the symbols for various values of the wave number k , together with the resulting fits to the expected analytical form (11), shown by the continuous curves.

density ripples of wave number k will be amplified at a rate $\gamma_k(\rho, \varepsilon)$. Its value depends on the strength of the gradient term and is given by the dispersion relation,

$$\gamma_k = \left[|v_s|^2 k^2 - a^2 \frac{\varepsilon_s}{h} \frac{\rho^2}{\rho_s^2} k^4 \right]^{\frac{1}{2}}. \quad (9)$$

The first term reflects the familiar linear rise obtained for standard ideal fluid dynamics, $\gamma_k = |v_s|k$, while the second term arises from the gradient term which introduces a penalty for the development of short-range undulations. As a consequence of these two opposing trends, the resulting growth rate γ_k exhibits a maximum at the favored length scale $\lambda_{\text{opt}} = 2\pi/k_{\text{opt}}$.

The spinodal growth rates can be extracted by following the time evolution of small harmonic perturbations of uniform matter. Thus, imposing periodic boundary conditions, we consider initial systems of the form

$$\rho(\mathbf{r}) = \bar{\rho} + \delta\rho(0) \sin(kx), \quad \varepsilon(\mathbf{r}) = \bar{\varepsilon} + \delta\varepsilon(0) \sin(kx), \quad (10)$$

where $(\bar{\rho}, \bar{\varepsilon})$ lies inside the spinodal phase region and the amplitudes $\delta\rho(0)$ and $\delta\varepsilon(0)$ are suitably small. Because the frequency is purely imaginary, $\omega_k = \pm i\gamma_k$, the early time evolution of the amplitudes will consist of growing and decaying exponentials having equal weights (because the initial state (10) is prepared without any flow) [39],

$$\delta\rho(t) \approx \delta\rho(0) \cosh(\gamma_k t), \quad \delta\varepsilon(t) \approx \delta\varepsilon(0) \cosh(\gamma_k t), \quad (11)$$

and it is then straightforward to extract the rate γ_k from the calculated amplitude growth.

This is illustrated in Fig. 3 for the phase point $(\bar{\rho}, \bar{\varepsilon}) = (6\rho_s, 10\varepsilon_s)$, which lies well inside the spinodal region, and using $(\delta\rho(0), \delta\varepsilon(0)) = (0.1\rho_s, 0.2\varepsilon_s)$. The subsequent

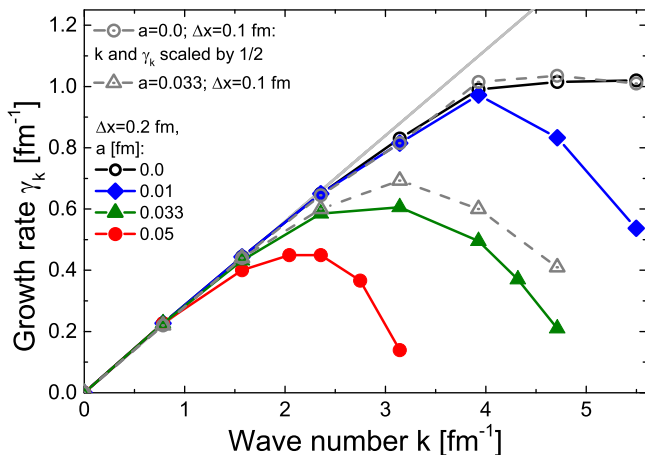


FIG. 4. [Color online] Spinodal dispersion relation γ_k , the growth rate as a function of the wave number. The straight line is the exact result for gradient-free ideal fluid dynamics, whereas the two top curves are the corresponding numerical results obtained with the standard grid size $\Delta x = 0.2$ fm (solid) or with $\Delta x = 0.1$ fm (dashed). The four lowest curves were obtained with finite values of the range a as indicated.

time evolution is obtained with ideal fluid-dynamics (without the gradient term for this illustration) and the Fourier components of the density are extracted. The resulting time-dependent amplitudes $\delta\rho_k(t)$ are then fitted with the analytical form (11). As the figure brings out, the expected form is indeed produced, indicating that the numerical propagation of the unstable system is reliable and that the growth rates γ_k can be extracted with confidence.

Figure 4 shows dispersion relations extracted in this manner for various scenarios. Ideal fluid dynamics without a gradient term yields the indicated straight line, $\gamma_k = |v_s|k$, and this behavior is indeed approached by the numerical results when the employed spatial grid size Δx is reduced: Our standard value of $\Delta x = 0.2$ fm yields the top solid curve, while using of half that value, $\Delta x = 0.1$ fm, simply scales up the resulting curve γ_k by a factor of two, *i.e.* $\gamma_{2k}[\frac{1}{2}\Delta x] = 2\gamma_k[\Delta x]$. The deviation of the numerical γ_k from the analytical behavior $|v_s|k$ is due to the numerical procedure in the SHASTA code [35].

The other curves on Fig. 4 have been calculated with the gradient term included, using the indicated values of the range a . They all lead to curves that exhibit a maximum growth rate and we see that using $\Delta x = 0.2$ fm ensures that the finite- a results are physically reasonable for range values down to $a = 0.01$ fm. Our studies suggest that while the gradient-free calculations with $\Delta x = 0.2$ fm are reliable only up to $k \lesssim 4/\text{fm}$ (beyond which the growth rate levels off towards a constant), the use of a finite range, $a > 0$, extends validity to significantly finer scales due to the suppression of such irregularities. Furthermore, for ranges above ≈ 0.01 fm the growth rates are rather insensitive to the

employed grid size Δx , as is illustrated for our standard range of $a = 0.033$ fm (which yields a surface tension of $\sigma_0 \approx 10$ MeV/fm², as discussed above).

In actual systems there is some degree of physical dissipation which gives rise to both viscosity and heat conduction. To leading order, the viscosity reduces the growth rate by $\approx \frac{1}{2}[\frac{4}{3}\eta + \zeta]k^2/h$, where η and ζ are the shear and bulk viscosity coefficients, respectively. But the heat conductivity generally increases the growth rate (in particular, it extends the boundary of the mechanically unstable region from the isentropic to the isothermal spinodal).

IV. NUCLEAR COLLISIONS

We have shown above that our model produces both meaningful interface properties, including the temperature-dependent strength of the associated tension, and reasonable spinodal growth rates, including the emergence of an optimal phase separation scale. The model is therefore suitable for addressing dynamical scenarios involving phase-transition instabilities.

For a first study, we have considered central collisions of lead nuclei bombarded onto a stationary lead target at various kinetic energies, E_{lab} . For each energy, an ensemble of several hundred separate evolutions are generated, each one starting from a different initial configuration generated by (the cascade mode of) the UrQMD model [40–42] which treats the non-equilibrium dynamics during the very early stage of the collision. The switch from UrQMD to fluid dynamics is made at the time

$$t_{\text{init}} = 2R/\sqrt{\gamma_{C.M.}^2 - 1}, \quad (12)$$

where $\gamma_{C.M.}$ is the center-of-mass frame Lorentz factor and R is the radius of the nucleus. At this time the two Lorentz-contracted nuclei have just passed through each other and all initial hard collisions have occurred. Each hadron is then represented by a gaussian of width $\sigma_{\text{init}} = 1$ fm and the needed fluid-dynamical quantities, $\rho(\mathbf{r})$, $\varepsilon(\mathbf{r})$, $\mathbf{u}(\mathbf{r})$, can then be extracted and tabulated on a desirable Cartesian spatial lattice [43]. In this way, the effects of stopping as well as local event-by-event fluctuations are automatically included in the ensemble of initial fluid-dynamic states.

A. Density clumping

The amplification of spatial irregularities presents an important effect of the presence of a first-order phase transition [22, 23, 25, 33]. In the present scenarios, spatial irregularities are present already in the initial state, whereas the fluid-dynamical propagation does not generate any spontaneous fluctuations in the course of the evolution (such fluctuations are generally produced at finite temperatures [44] but this refinement has not yet been incorporated into the fluid-dynamical transport treatments of nuclear collisions).

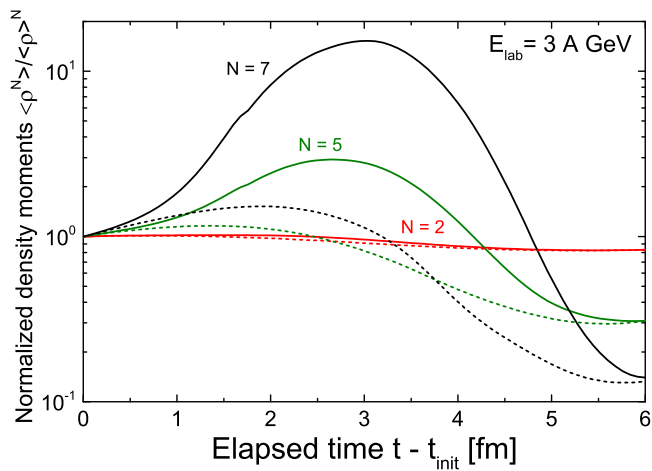


FIG. 5. [Color online] Mean time evolution of the amplification of normalized density moments obtained for $E_{\text{lab}} = 3A$ GeV with $a = 0.033$ fm (for which $\sigma_0 \approx 10$ MeV/fm²), using either the two-phase equation of state (solid) or its one-phase partner (dashed).

For any given event, and at any given time, parts of the system may lie within the unstable or metastable region, and local density irregularities may then become amplified, whereas the rest of the matter is situated in a stable phase region where irregularities tend to erode. In order to ascertain the effect of those instabilities, we also carry out corresponding simulations with the one-phase Maxwell partner equation of state which contains no instabilities but is otherwise identical.

A convenient quantitative measure of the resulting degree of “clumping” in the system is provided by the moments of the baryon density density $\rho(\mathbf{r})$,

$$\langle \rho^N \rangle \equiv \frac{1}{A^N} \int \rho(\mathbf{r})^N \rho(\mathbf{r}) d^3\mathbf{r}, \quad (13)$$

where $A = \int \rho(\mathbf{r}) d^3\mathbf{r} = \langle \rho^0 \rangle$ is the total (net) baryon number. The corresponding normalized moments, $\langle \rho^N \rangle / \langle \rho \rangle^N$, are dimensionless and increase with the order N , for a given density distribution $\rho(\mathbf{r})$; the normalized moment for $N = 1$ is unity.

The time evolution of the amplification of the normalized density moments is illustrated in Fig. 5 for $N = 2, \dots, 7$, as obtained with both equations of state. The two sets of results differ strikingly: Whereas the one-phase equation of state hardly produces any amplification at all, the one having a phase transition leads to significant enhancements, amounting to well over an order of magnitude for $N = 7$. This clearly demonstrates that the first-order phase transition may have a qualitative influence on the dynamical evolution of the density. Due to the variations in the initial conditions, the phase regions explored differ from one collision to the other. As a result, some of the evolutions experience amplifications that are significantly larger than the ensemble average (by up to a factor of five or so), whereas more evolutions

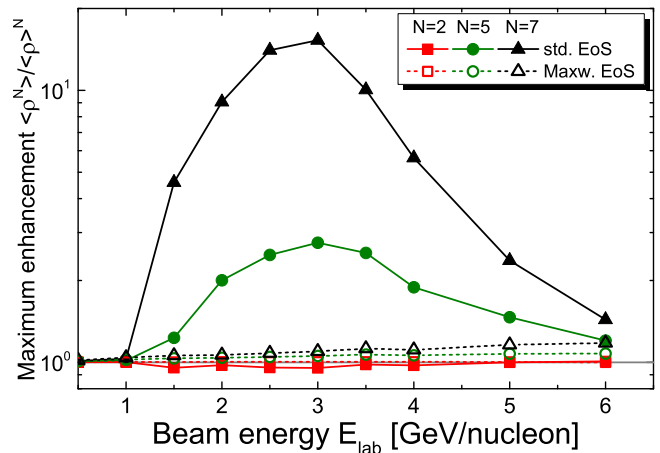


FIG. 6. [Color online] Mean maximum enhancement of the normalized density moments for $N=7, 5$ (squares, circles) as obtained for various energies using either the two-phase equation of state (solid) or its one-phase Maxwell partner (dashed).

are affected considerably less.

Figure 5 depicts what would happen if the expansion were to continue while maintaining local equilibrium so the generated density enhancements eventually subside. However, as the hadronic gas grows more dilute, local equilibrium cannot be maintained. Consequently, if the decoupling occurs sufficiently soon after the clumps are formed, the associated phase-space correlations may survive. Such a correlation might be observed in a change of the width of two particle correlation functions [45], even after the hadronic rescattering. This issue requires more detailed studies which are underway.

The degree of density clumping generated during a collision depends on how long time the bulk of the matter is exposed to the spinodal instabilities. The optimal situation occurs for collision energies that produce maximum bulk compressions lying well inside the unstable phase region because the instabilities may then act for the longest time [25, 32, 33]. At lower energies an ever smaller part of the system reaches instability and the resulting enhancements are smaller. Conversely, at higher energies the maximum compression occurs beyond the spinodal phase region and the system is exposed to the instabilities only during a relatively brief period during the subsequent expansion. For still higher energies the spinodal region is being missed entirely.

Figure 6 shows the (ensemble average) maximum enhancement achieved as a function of the beam energy for the two equations of state. The existence of an optimal collision energy is clearly brought out. While the presently employed equation of state suggests that this optimal range is $E_{\text{lab}} \approx 2 - 4$ A GeV, it should be recognized that others may lead to different results. Furthermore, the magnitude of the effect depends on the degree of fluctuation in the initial conditions which in turn are governed by the pre-equilibrium dynamics. On the

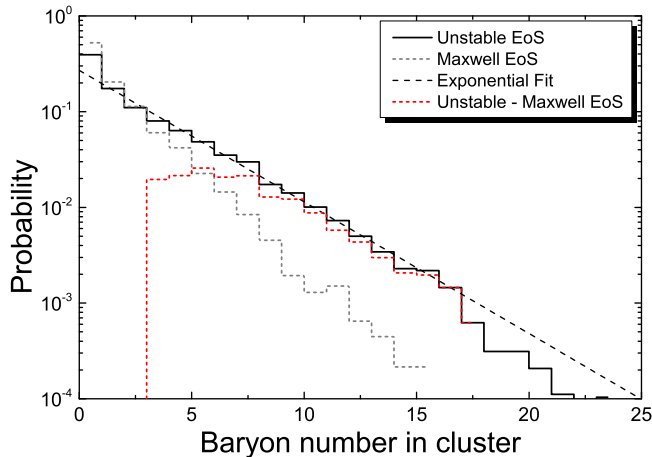


FIG. 7. The size distribution of the density clumps produced in central lead-lead collisions at 3 A GeV using $\rho_{\min} = 7\rho_s$ to define the clump boundary. The solid histogram shows the distribution obtained for the two-phase equation of state and the solid line represents an exponential fit. The distribution obtained with the one-phase equation of state is shown by the dotted histogram and the difference between the two size distributions is also depicted.

other hand, our studies suggest that the optimal energy is rather insensitive to the range parameter a .

B. Size distribution

To gain a more detailed understanding of the clumping phenomenon, we have studied the distribution of the clump sizes. Although the “clumps” tend to remain fairly diffuse, we may define their extension by means of a specified density cutoff, ρ_{\min} , and then extract the total net baryon number contained within the resulting volume. Figure 7 shows the size distribution obtained for a density cutoff of $\rho_{\min} = 7\rho_s$, for central lead-lead collisions at 3 A GeV.

The initial size distribution is approximately exponential and that feature is well preserved during the evolution with the one-phase equation of state which produces negligible amplification. The spinodal instabilities in the two-phase equation of state leads to a preferential amplification of length scales near the optimum size, as is brought out by the difference between the two-phase size-distribution and the one obtained with the Maxwell partner; this difference peaks at clumps containing 5-8 baryons. Nevertheless, for a wide intermediate range, from about 3 to about 16, the resulting two-phase size distribution retains an approximately exponential appearance, but with a significantly gentler slope.

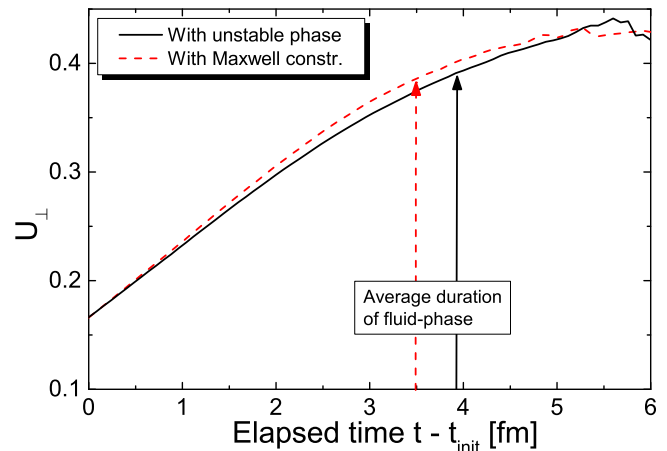


FIG. 8. (Color online) The time evolution of the average transverse flow velocity U_{\perp} for central lead-lead collisions at a fixed-target beam kinetic energy of $E_{\text{lab}} = 3$ A GeV for the two-phase equation of state (solid) and its one-phase Maxwell partner (dashed). The arrows indicate the average completion of the fluid-dynamical stage, defined as the time when all fluid cells have energy densities below five times the nuclear ground-state energy density.

C. Transverse Flow

Radial flow has long been thought to be affected the presence of a first-order phase transition because of the accompanying softening of the equation of state [46]. It may therefore be expected that the transverse flow exhibits a corresponding weakening. However, recent investigations using state-of-the-art dynamical models suggest that a simple connection between the softening of the equation of state and the radial flow (and its angular moments) cannot so easily be drawn [47, 48]. Although a softer equation of state does reduce the build up of flow, it also leads to a longer expansion time which tends to have an opposite effect.

We investigate here the effect of the phase transition on the transverse flow to determine whether it may serve as a useful signal. For this purpose, we define the transverse flow velocity U_{\perp} as

$$U_{\perp}(t) = \frac{1}{M(t)Q(t)} \int [v_x(\mathbf{r}, t)x + v_y(\mathbf{r}, t)y] \rho(\mathbf{r}, t) d^3\mathbf{r}, \quad (14)$$

where $\rho(\mathbf{r})$ is the local (net) baryon density at the position $\mathbf{r} = (x, y, z)$, while $v_x(\mathbf{r})$ and $v_y(\mathbf{r})$ are the transverse components of the local fluid velocity $\mathbf{v}(\mathbf{r})$. M and Q are defined as follows,

$$M(t) = \int \rho(\mathbf{r}, t) d^3\mathbf{r}, \quad (15)$$

$$M(t)Q(t)^2 = \int [x^2 + y^2] \rho(\mathbf{r}, t) d^3\mathbf{r}. \quad (16)$$

Figure 8 shows our results for the average transverse

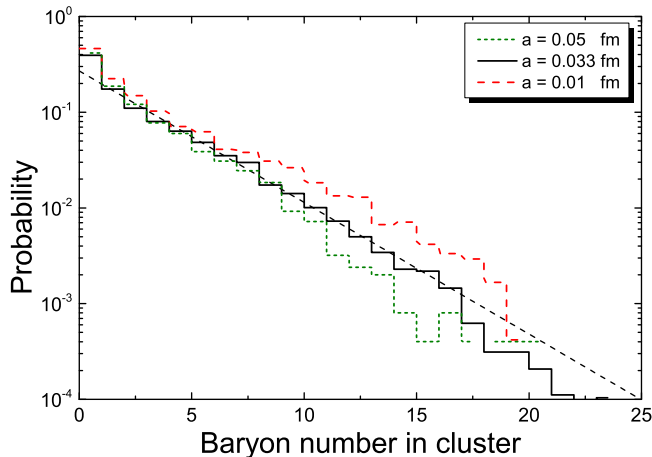


FIG. 9. (Color online) The size distribution of the density clumps produced in central lead-lead collisions at 3 A GeV as obtained for various values of the range parameter a with the two-phase equation of state. The dashed line shows an exponential fit to the standard result (obtained for $a = 0.033$ fm)

flow of baryons as a function of time for central lead-lead collisions at the fixed-target beam energy of $E_{\text{lab}} = 3.4$ GeV for which the density moments exhibited their largest enhancement. Indeed transverse flow builds up more slowly for the two-phase equation of state than for its one-phase Maxwell partner, though the difference between the two cases is very small, probably too small to be of experimental utility. Furthermore, the larger stiffness of the one-phase equation of state causes the expansion to be faster, so the end of the fluid-dynamical stage (the time when the energy density has become sufficiently low, $\varepsilon = 5\varepsilon_s$ in the present case) will occur sooner and this shorter expansion time will largely offset the (small) gain in flow velocity. As a result, the average transverse flow velocities become almost identical at the end of the fluid-dynamical stage. Consequently, this quantity does not seem promising as a signal for the phase transition.

V. PARAMETER STUDIES

The fluid dynamical model employed has several parameters that are not well constrained by our current knowledge of QCD. These include the strength of the interface tension, the spatial scale of the initial density irregularities, and the equation of state of baryon-rich uniform matter. In the following, we investigate the dependence of our results on these quantities by varying the respective controlling parameters one at a time.

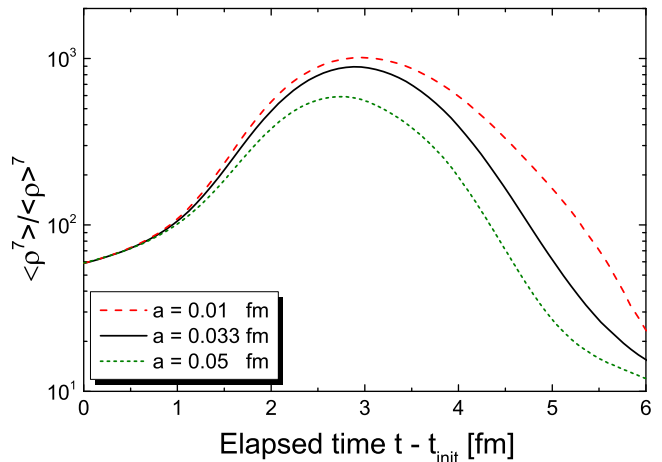


FIG. 10. (Color online) The time evolution of the seventh normalized density moment for central lead-lead collisions at $E_{\text{lab}} = 3.4$ GeV for three different values of the range parameter a , using the standard value $\sigma_{\text{init}} = 1$ fm for the spatial scale of the initial density irregularities.

A. Finite range

Figure 9 shows the dependence of the clump size distribution on the range parameter a governing the interface tension between baryon-rich confined and deconfined matter, for the optimal collision energy. We have shown above that density irregularities in the unstable phase region will grow faster for smaller ranges. This feature is also reflected in the size distribution: a smaller a value enhances the yield of larger clumps (*i.e.* density enhancements with larger baryon contents) and, conversely, a larger a value decreases the large- A yield.

Figure 10 shows how the variation in the range parameter a affects the time dependence of the seventh normalized density moment. As expected, a smaller value of the range a leads to a stronger enhancement of irregularities, as already brought out in figure 9.

B. Initial fluctuations

Figure 11 shows the dependence of the size distribution on the parameter σ_{init} characterizing the spatial scale of the initial density irregularities. Although a reduction of the scale from the standard value of $\sigma_{\text{init}} = 1$ fm shifts the clump sizes to larger values, the difference between the cases of $\sigma_{\text{init}} = 0.7$ fm and $\sigma_{\text{init}} = 0.5$ fm is very small, indicating that the fluctuation growth saturates when the scale of the initial irregularities is reduced.

Figure 12 shows how the reduction of σ_{init} affects the evolution of the seventh normalized density moment. The behavior is somewhat complicated. While the initial value of the moment increases when the fluctuation scale σ_{init} is reduced, its relative growth tends to become smaller. This feature may be ascribed to the fact

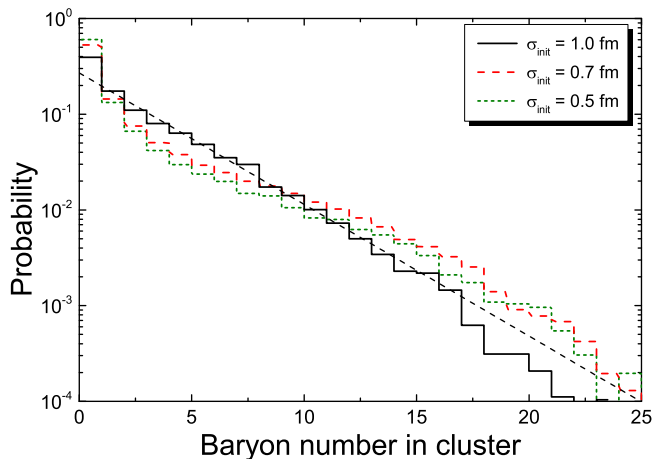


FIG. 11. (Color online) The size distribution of the clumps produced in central lead-lead collisions at 3 A GeV obtained for different values of the parameter σ_{init} controlling the spatial scale of the initial irregularities, using $a = 0.033$ fm and the two-phase equation of state. The dashed line shows an exponential fit to the standard result (obtained for $\sigma_{\text{init}} = 1$ fm).

that a system with larger initial density fluctuations also has larger density gradients, which in turn implies that also a smaller part of the system lies inside the unstable phase region. Furthermore, the larger gradients also cause the expansion through the unstable coexistence region to proceed more rapidly.

For our present studies, the initial state of the fluid-dynamical evolution has been obtained by use of the UrQMD model in its cascade mode in which there are neither inter-nuclear potentials nor nuclear mean fields. However, for nuclear collisions at the relatively low energies of relevance here, below $E_{\text{lab}} \approx 5 - 10$ A GeV, a realistic description of the nuclear interactions is important for describing observables like the elliptic or directed flow [49]. An UrQMD treatment of the initial state that includes mean-field type nuclear interactions [50] will decrease the initial compression of the fireball.

Figure 13 compares the maximum enhancements of the fifth and seventh normalized density moments obtained with the cascade-mode initial conditions used in the present study with those obtained when nuclear interactions are included. It is obvious that an enhancement is obtained only when the initial density has been generated in the cascade mode. This can be understood as a result of the considerably decreased initial compression due to the nuclear repulsive force which prevents the bulk of the system achieving the compressions characteristic of the unstable phase region.

The results bring out the fact that the degree of density enhancement caused by the phase transition depend strongly on the initial compression relative to the location of the unstable region in the phase diagram. The discussions on the mean-field effect on the initial conditions are based on the hadronic mean fields in the UrQMD model,

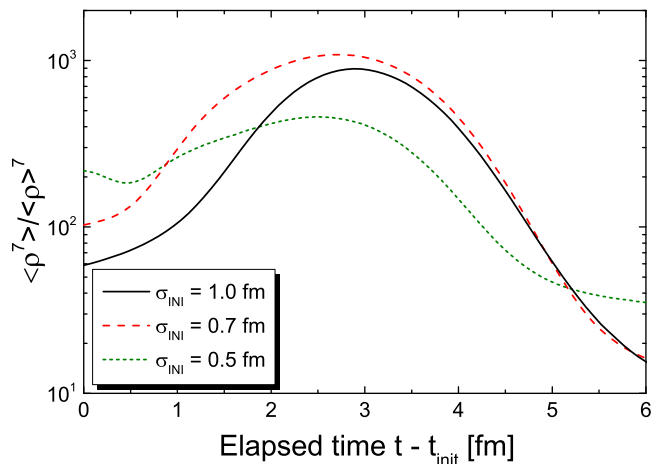


FIG. 12. (Color online) The time evolution of the seventh normalized moment for central lead-lead collisions at 3A GeV for three different values of the parameter σ_{init} controlling the scale of the initial density fluctuations, using $a = 0.033$ fm.

which are strongly repulsive when the baryon density is large. Since the initial state in the present study is a baryon-rich quark matter, the mean fields in such a matter may be different from those in hadronic matter. For example, the quark mean-field in the NJL model is attractive due to the strong attractive scalar part (see Song et al. [51] and references therein).

C. Equation of State

To further illuminate this latter feature, we now modify the equation of state and investigate the dependence of the results on the location of the unstable region.

For this purpose, we consider a family of equations of state obtained by rescaling the basic mechanical densities ε and ρ . Thus, a particular scaled equation of state has the entropy density $\sigma_{bc}(\varepsilon, \rho) \doteq \sigma_0(b\varepsilon, c\rho)$, where $\sigma_0(\varepsilon, \rho)$ is the entropy density of our standard equation of state. It is then readily shown that the associated temperature and chemical potential are given by

$$T_{bc}(\varepsilon, \rho) = \frac{1}{b}T_0(b\varepsilon, c\rho), \quad \mu_{bc}(\varepsilon, \rho) = \frac{c}{b}\mu_0(b\varepsilon, c\rho), \quad (17)$$

where $T_0(\varepsilon, \rho) = 1/\partial_\varepsilon\sigma_0(\varepsilon, \rho)$ is the temperature of the standard equation of state, while the corresponding chemical potential is $\mu_0(\varepsilon, \rho) = -T_0(\varepsilon, \rho)/\partial_\rho\sigma_0(\varepsilon, \rho)$. It follows that the pressure $p = T\sigma - \varepsilon + \mu\rho$ is given by

$$p_{bc}(\varepsilon, \rho) = \frac{1}{b}p_0(b\varepsilon, c\rho). \quad (18)$$

The enthalpy and the free energy scale similarly, *i.e.* $h_{bc}(\varepsilon, \rho) = h_0(b\varepsilon, c\rho)/b$ and $f_{bc}(\varepsilon, \rho) = f_0(b\varepsilon, c\rho)/b$. It is also easy to see that the compressibilities remain invariant, $c_v^{bc}(\varepsilon, \rho) = c_v^0(b\varepsilon, c\rho)$ and $c_p^{bc}(\varepsilon, \rho) = c_p^0(b\varepsilon, c\rho)$.

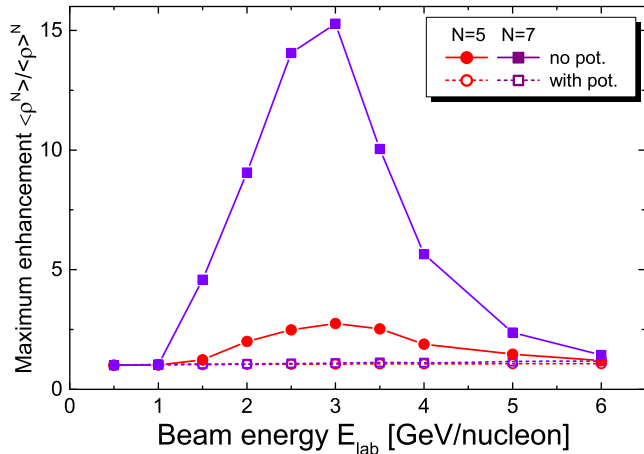


FIG. 13. (Color online) The collision energy dependence of the average maximum enhancement of the normalized density moments for $N = 7, 5$ as obtained for initial states generated either by the cascade mode of the UrQMD model (our standard) or with the inclusion of mean fields.

The same holds for the sound speeds,

$$v_s^{bc}(\varepsilon, \rho) = v_s^0(b\varepsilon, c\rho), \quad v_T^{bc}(\varepsilon, \rho) = v_T^0(b\varepsilon, c\rho), \quad (19)$$

thus ensuring that the isentropic and isothermal spinodal boundaries stretch in proportion to the employed scale factors. In particular, the scaled critical point is given by $(\varepsilon_{bc}^{\text{crit}}, \rho_{bc}^{\text{crit}}) = (\varepsilon_0^{\text{crit}}/b, \rho_0^{\text{crit}}/c)$.

The scaling properties exhibited above provides a convenient means for exploring different equations of state. As an illustration, Fig. 14 compares the energy dependence of the density enhancements obtained with our standard equation of state to those obtained with an equation of state that has been stretched upwards by 30% in both directions, *i.e.* $b = 1/1.3$ and $c = 1/1.3$. We see that the qualitative features remain very similar. In particular, there is still an optimal collision energy. The larger enhancement obtained for the scaled equation of state is primarily due to the corresponding expansion of the unstable phase region which allows the amplification to proceed for a longer time. However, the optimal collision energy is only slightly increased.

VI. SUMMARY

As reported recently [32], we have augmented an existing finite-density ideal fluid dynamics code with a gradient term and thereby obtained a transport model that is suitable for simulating nuclear collisions in the presence of a first-order phase transition. It describes both the temperature-dependent tension between coexisting phases and the amplification of the spinodal modes. Applying this novel model to lead-lead collisions, using an

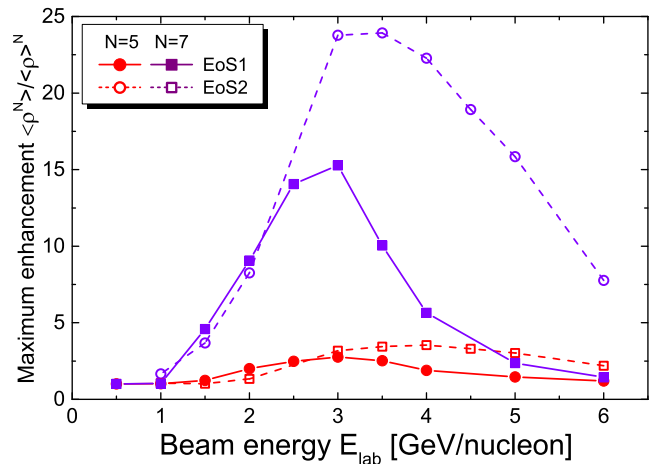


FIG. 14. (Color online) The average maximum enhancement of the normalized density moments for $N = 7, 5$ as a function of the beam kinetic energy E_{lab} , obtained with either our standard equation of state (solid curves) or the scaled one corresponding to $b = 1/1.3$ and $c = 1/1.3$ (dashed curves).

equation of state with a first-order phase transition, we found that the associated instabilities may cause significant amplification of initial density irregularities, relative to what would be obtained without the phase transition. Because such clumping may give rise to observable effects that could signal the presence of the phase transition, perhaps through enhanced composite-particle production, it is interesting to explore this phenomenon in more detail.

We have here given a more detailed account of this novel simulation tool and carried out more exhaustive studies of the phase-separation dynamics. In particular, we extracted the density enhancement, the clump size distribution, and the transverse flow velocity and examined the sensitivity of these quantities to the strength of the gradient term that promotes the phase separation, to the details of the initial density fluctuations that form the seeds for the subsequent amplification, and to the equation of state, all quantities that are yet not very well understood. We found that our results are robust against moderate changes of these model parameters.

While the presence of a phase transition greatly increases the density enhancements, it has only little effect on the resulting transverse flow. Perhaps most importantly, studies using different equations of state support the general existence of an optimal collision energy range within which the phase-transition instabilities have the largest effects on the dynamical evolution. Our results suggest that this energy corresponds to several GeV per nucleon of kinetic energy for a fixed-target configuration, a range that may be too low to access effectively at RHIC but which should match well with both FAIR and, especially, NICA.

VII. ACKNOWLEDGMENTS

We wish to acknowledge stimulating discussion with Volker Koch. This work was supported by the Office of

Nuclear Physics in the U.S. Department of Energy's Office of Science under Contract No. DE-AC02-05CH11231; JS was supported in part by the Alexander von Humboldt Foundation as a Feodor Lynen Fellow.

-
- [1] S.V. Afanasiev *et al.* [NA49 Collaboration], Phys. Rev. C **66**, 054902 (2002)
- [2] M. Gazdzicki *et al.* [NA49 Collaboration], J. Phys. **G30**, S701 (2004)
- [3] L. Kumar [STAR Collaboration], J. Phys. **G38**, 124145 (2011)
- [4] J. Adams *et al.* [STAR Collaboration], Nucl. Phys. A **757**, 102 (2005)
- [5] B.B. Back *et al.*, Nucl. Phys. A **757**, 28 (2005)
- [6] I. Arsene *et al.* [BRAHMS Collaboration], Nucl. Phys. A **757**, 1 (2005)
- [7] K. Adcox *et al.* [PHENIX Collaboration], Nucl. Phys. A **757**, 184 (2005)
- [8] K. Aamodt [ALICE Collaboration], Phys. Rev. Lett. **106**, 032301 (2011)
- [9] K. Aamodt [ALICE Collaboration], Phys. Lett. B **696**, 30 (2011)
- [10] K. Aamodt [ALICE Collaboration], Phys. Rev. Lett. **105**, 252302 (2010)
- [11] B. Abelev [ALICE Collaboration], Phys. Rev. Lett. **105**, 252301 (2010)
- [12] M.A. Stephanov, K. Rajagopal, and E.V. Shuryak, Phys. Rev. Lett. **81**, 4816 (1998)
- [13] S. Borsanyi *et al.*, JHEP **1011**, 077 (2010)
- [14] A. Bazavov and P. Petreczky [HotQCD collaboration], J. Phys. Conf. Ser. **230**, 012014 (2010)
- [15] Z. Fodor and S.D. Katz, JHEP **0203**, 014 (2002)
- [16] Z. Fodor and S.D. Katz, JHEP **0404**, 050 (2004)
- [17] P. de Forcrand and O. Philipsen, JHEP **0811**, 012 (2008)
- [18] G. Endrodi, Z. Fodor, S.D. Katz, and K.K. Szabo, JHEP **1104**, 001 (2011)
- [19] B.I. Abelev *et al.*, Internal STAR Note SN0493, 2009: drupal.star.bnl.gov/STAR/starnotes/public/sn0493.
- [20] B. Friman, C. Höhne, J. Knoll, S. Leupold, J. Randrup, R. Rapp, and P. Senger, *The CBM Physics Book*, (Springer, Berlin, 2010).
- [21] A.N. Sissakian and A.S. Sorin, J. Phys. G **36**, 064069 (2009).
- [22] Ph. Chomaz, M. Colonna, and J. Randrup, Phys. Rep. **389**, 263 (2004).
- [23] J. Randrup, Phys. Rev. Lett. **92**, 122301 (2004)
- [24] C. Sasaki, B. Friman, and K. Redlich, Phys. Rev. Lett. **99**, 232301 (2007)
- [25] J. Randrup, Phys. Rev. C **79**, 054911 (2009)
- [26] J. Randrup, Acta Phys. Hung. A **22**, 69 (2005).
- [27] V. Koch, A. Majumder, and J. Randrup, Phys. Rev. C **72**, 064903 (2005).
- [28] I.N. Mishustin, Phys. Rev. Lett. **82**, 4779 (1999)
- [29] D. Bower and S. Gavin, Phys. Rev. C **64**, 051902 (2001)
- [30] K. Paech, H. Stöcker, and A. Dumitru, Phys. Rev. C **68**, 044907 (2003)
- [31] M. Nahrgang, S. Leupold, C. Herold, and M. Bleicher, Phys. Rev. C **84**, 024912 (2011).
- [32] J. Steinheimer and J. Randrup, Phys. Rev. Lett. **109**, 212301 (2012).
- [33] J. Randrup, Phys. Rev. C **82**, 034902 (2010)
- [34] B. Borderie *et al.*, Phys. Rev. Lett. **86**, 3252 (2001).
- [35] D.H. Rischke, S. Bernard and J.A. Maruhn, Nucl. Phys. A **595**, 346 (1995)
- [36] B.W. Mintz, R.O. Ramos, J. Schaffner-Bielich, and R. Stiele, arXiv:1212.1184 [hep-ph].
- [37] H. Heiselberg, C.J. Pethick, and E.F. Staubo, Phys. Rev. Lett. **70**, 1355 (1993).
- [38] D.N. Voskresensky, M. Yasuhira, and T. Tatsumi, Nucl. Phys. A **723**, 291 (2003).
- [39] M. Colonna, Ph. Chomaz, and J. Randrup, Nucl. Phys. A **567**, 637 (1994).
- [40] S.A. Bass *et al.*, Prog. Part. Nucl. Phys. **41**, 255 (1998) [Prog. Part. Nucl. Phys. **41**, 225 (1998)]
- [41] M. Bleicher *et al.*, J. Phys. **G25**, 1859 (1999)
- [42] H. Petersen, J. Steinheimer, G. Burau, M. Bleicher, and H. Stöcker, Phys. Rev. C **78**, 044901 (2008)
- [43] J. Steinheimer, M. Bleicher, H. Petersen, S. Schramm, H. Stöcker, and D. Zschesche, Phys. Rev. C **77**, 034901 (2008)
- [44] J.I. Kapusta, B. Müller, and M. Stephanov, Phys. Rev. C **85**, 054906 (2012)
- [45] L. -W. Chen, C. M. Ko, W. Liu and B. -W. Zhang, PoS CPOD **2009**, 034 (2009)
- [46] L. Van Hove, Phys. Lett. B **118**, 138 (1982).
- [47] H. Petersen, J. Steinheimer, M. Bleicher, and H. Stöcker, J. Phys. **G36**, 055104 (2009)
- [48] J. Steinheimer, V. Dexheimer, H. Petersen, M. Bleicher, S. Schramm, and H. Stöcker, Phys. Rev. C **81**, 044913 (2010)
- [49] H. Petersen, Q. Li, X. Zhu, and M. Bleicher, Phys. Rev. C **74**, 064908 (2006)
- [50] Q.F. Li, Z.X. Li, S. Soff, M. Bleicher, and H. Stöcker, J. Phys. **G32**, 407 (2006)
- [51] T. Song, S. Plumari, V. Greco, C. M. Ko and F. Li, arXiv:1211.5511 [nucl-th].